Available online at www.sciencedirect.com

SciVerse ScienceDirect

Proceedings of the Combustion Institute 34 (2013) 1231–1239

Proceedings of the Combustion Institute

www.elsevier.com/locate/proci

Subgrid-scale mixing of mixture fraction, temperature, and species mass fractions in turbulent partially premixed flames

Shuaishuai Liu, Chenning Tong *

Department of Mechanical Engineering, Clemson University, Clemson, SC 29634-0921, USA

Available online 15 June 2012

Abstract

The subgrid-scale (SGS) mixing of mixture fraction, temperature, and species mass fraction in turbulent partially premixed (Sandia) flames is studied. We focus on the effects of the SGS mixing regimes and the spatial relationships among the scalars on the SGS mixing of the species mass fractions. High-resolution lines images are used to obtain the scalar filtered mass density function and the conditionally filtered diffusion. The results show that for small SGS variance the scalar fields have a relatively simple structure. For large SGS variance the structure is more complex. The spatial relationships among the scalars result in different SGS scalar structures and SGS mixing characteristics, with the mass fraction of CO_2 being the simplest and that of CO being the most complex. The results in this study present a challenging test for SGS mixing models.

Keywords: Turbulent flames; Large-eddy simulation; Filtered density function; Turbulent mixing

1. Introduction

Turbulent mixing and turbulence-chemistry interaction are key processes that must be accurately accounted for in turbulent combustion models. In large-eddy simulation (LES) of turbulent combustion, mixing by the large, resolved scales is computed. The effects of the subgrid scales, including the subgrid-scale (SGS) scalar mixing and the resulting instantaneous distribution of scalar values in each grid volume, i.e., the species filtered joint mass density function (FMDF), are modeled [1,2]. Modeling the FMDF, therefore, is the main challenge in LES and requires knowledge of SGS mixing and its interaction with chemistry.

Our previous studies [3–8] have shown that SGS mixing of the mixture fraction has two regimes depending on the *instantaneous* SGS scalar variance. When the SGS variance is small compared to its mean value, the distribution of the SGS scalar is close to Gaussian, indicating well mixed SGS scalar fields. This regime generally supports distributed reaction zones. When the SGS variance is large compared to its mean value, the distribution is bimodal, indicating highly non-premixed SGS scalar fields, i.e., the fuel lean and rich regions of the SGS fields in a flame are highly segregated. There is a sharp interface (cliff) separating the two regions. This regime generally supports flamelets. The conditional SGS scalar structure resembles that of a counter-flow diffusion flame, which is a model for laminar flamelets.

The well-mixed and the highly-nonpremixed SGS mixture fraction mixing regimes have strong

* Corresponding author. Fax: +864 6564435.
E-mail address: ctong@clemson.edu (C. Tong).

1540-7489/$ - see front matter © 2010 The Combustion Institute. Published by Elsevier Inc. All rights reserved.
http://dx.doi.org/10.1016/j.proci.2012.05.017

influences on SGS mixing of reactive scalars. Cai et al. [9] studied the effects of the SGS mixing regimes on the SGS mixing of the temperature in the Sandia flames. It was found that for small SGS scalar variance, the conditionally filtered diffusion of the mixture fraction and temperature for the burning samples, represented by streamlines, generally move towards the ridgeline of the FMDF and then move along it towards a stagnation point. Mixing between burning and extinguished samples generally causes the streamlines to converge to another stagnation point at a lower temperature. The SGS mixing of the temperature has some characteristics similar to those of a non-reactive scalar. For large SGS scalar variance, the mixing process is more complex. The streamlines not far from the equilibrium are consistent with flamelets. The samples at lower temperatures are largely due to extinguished flamelets, which initially cause the streamlines to move predominately in the direction of the mixture fraction and then in the direction of temperature toward a stagnation point. The latter is likely due to diffusion along the iso-mixture fraction surfaces among burning and extinguished flamelets. These results show that it is important for mixing models to be able to account for these SGS mixing processes.

In this study we investigate the effects of the SGS mixture fraction structure on the conditionally filtered scalar diffusion, temperature diffusion, and species mass fraction diffusion in turbulent partially premixed flames, which evolve the FMDF of mixture fraction, temperature, and species mass fractions:

$$\begin{aligned} F_{\xi TY_i}(\hat{\xi},\hat{T},\hat{Y}_i;\mathbf{x},t) &= \langle \rho(\mathbf{x},t)\delta(\xi-\hat{\xi})\delta(T-\hat{T})\delta(Y_i-\hat{Y}_i)\rangle_\ell \\ &= \int \rho(\mathbf{x}',t)\delta(\xi-\hat{\xi})\delta(T-\hat{T})\delta(Y_i-\hat{Y}_i) \\ &\quad \times G(\mathbf{x}-\mathbf{x}')d\mathbf{x}', \end{aligned} \tag{1}$$

where ξ, T, Y_i, $\hat{\xi}$, $\hat{T}$ and $\hat{Y}_i$ are the mixture fraction, temperature, species mass fraction and their sample-space variables, respectively, and ρ is the fluid density. The filter function is denoted by G. The subscripts ℓ and L denote conventional and Favre filtered variables, respectively. The knowledge of these diffusion terms is important for understanding SGS mixing of multiple reactive scalars and the SGS turbulence-chemistry interaction.

2. Experimental data and processing procedures

We use experimental data obtained in piloted turbulent partially premixed methane flames with a 1:3 ratio of CH_4 to air by volume (Sandia flames D and E, see Ref. [10,11]). The measurements employed combined line-imaging of Raman scattering, Rayleigh scattering, and laser-induced CO fluorescence. Simultaneous measurements of the major species (CO_2, O_2, CO, N_2, CH_4, H_2O, and H_2), the mixture fraction (obtained from all major species), and the temperature were made. The mixture fraction is calculated using a variation of Bilger's definition, which has been modified by excluding the oxygen terms. The length of the imaging line is 6.13 mm with a pixel resolution of 0.2044 mm. The overall resolution of the imaging system is capable of resolving 98% of the highest scalar dissipation [12].

Measurements of the filtered density functions (FDF) require spatial filtering of scalar fields. In this work one-dimensional filtering is employed. In LES filtering is generally performed in three dimensions. The conditional FDF is formally a one-point statistic, and does not depend on the dimensionality of the data (and filter). Indeed, our previous results [5] have shown that the FDF obtained using a one-dimensional filter is qualitatively the same as those using a two-dimensional filter. The main effect of a one-dimension filter is a somewhat higher SGS variance, which affect the conditional FDF. The increase in the SGS variance also affects the conditionally filtered scalar diffusion. This increase, however, is not sufficiently large to significantly alter the FDF and the conditionally filtered scalar diffusion. Small-scale anisotropy can also result in differences between the scalar diffusion obtained using one- and three-dimensional data. Given the moderate level of anisotropy in free shear flows, however, we expect the one-dimensional results to be good approximations of three-dimensional results. To ensure that the results are relevant to LES at high Reynolds numbers, the filter sizes employed in this work (3.0 mm and 4.9 mm) are significantly larger than the dissipative (Corrsin) scales (0.065–0.106 mm [13]), so that the subgrid scales contain sufficient fluctuations, allowing the physics of the SGS mixing and its interaction with the chemistry to be related to the inertial-range dynamics. Given the moderate Reynolds number of the Sandia flames, the filter sizes employed are not very small compared to the integral length scales. Nevertheless, they are more preferable than smaller filter sizes, which will not be much larger than the Corrsin scale. Previous studies (e.g., Refs. [3,5]) have shown that when the filter size is much larger than the dissipation scales the properly scaled conditional statistics are not sensitive to the filter size.

3. Results

In this section the FMDF and the conditionally filtered diffusion of the mixture fraction, temperature, and species mass fractions are analyzed using their conditional means. We use the Favre

filtered mixture fraction, $\langle\xi\rangle_L = \langle\rho\xi\rangle_\ell / \langle\rho\rangle_\ell$, and the Favre SGS scalar variance,

$$\langle\xi''^2\rangle_L \equiv \frac{1}{\langle\rho\rangle_\ell}\int F_{\xi L}(\hat{\xi};\mathbf{x},t)(\xi - \langle\xi\rangle_L)^2 d\xi = \langle\rho\xi^2\rangle_\ell/\langle\rho\rangle_\ell - \langle\xi\rangle_L^2, \quad (2)$$

as conditioning variables. The filtered mixture fraction, $\langle\xi\rangle_L$, is set to the stoichiometric mixture fraction, ξ_s(=0.35), to maximize the probability of the SGS fields containing reaction zones. At each measurement location, two SGS variance values, one small and one large (much smaller and much larger than the mean SGS variance respectively), are chosen to sample SGS fields representing the two limiting SGS mixing regimes. For the flame studied, the percentage contributions to the scalar dissipation rate in the reaction zones (the approximate heat release rate) from distributed reaction zones and flamelet regimes are approximately 55% and 45%, respectively [8].

To achieve reasonable statistical convergence for the FMDF and the conditionally filtered diffusion for all the major species, a data sample size much larger than the current set is needed. Thus, in this study we include one major species at a time, i.e., we consider the FMDF of the mixture fraction, the temperature, and one species mass fraction and the related SGS mixing terms in the FMDF transport equation. Using the analysis described in [14], the maximum rms uncertainty of the FMDF obtained are determined to be approximately 10% of the peak FMDF values, comparable to the uncertainty in the species data [15]. To fully represent the FMDF and the SGS mixing terms, a three-dimensional scalar space is needed. We present them as functions of the three sample-space variables.

The conditionally filtered diffusion of the mixture fraction, the temperature, and a species mass fraction, $\left\langle\left\langle\frac{1}{\rho}\frac{\partial}{\partial y}\left(\rho D\frac{\partial\xi}{\partial y}\right)\middle|\xi,T,Y_i\right\rangle_\ell\middle|\langle\xi\rangle_L, \langle\xi''^2\rangle_L\right\rangle$, $\left\langle\left\langle\frac{1}{\rho}\frac{\partial}{\partial y}\left(\rho D_T\frac{\partial T}{\partial y}\right)\middle|\xi,T,Y_i\right\rangle_\ell\middle|\langle\xi\rangle_L,\langle\xi''^2\rangle_L\right\rangle$, and $\left\langle\left\langle\frac{1}{\rho}\frac{\partial}{\partial y}\left(\rho D\frac{\partial Y_i}{\partial y}\right)\middle|\xi,T,Y_i\right\rangle_\ell\middle|\langle\xi\rangle_L,\langle\xi''^2\rangle_L\right\rangle$, respectively, appear in the FMDF equation as terms transporting the FMDF in the ξ, T, and Y_i spaces, respectively. Thus, they are the three components of the diffusion velocity of the FMDF in the sample space. We use streamlines and isocontours to present the direction and the magnitude of the diffusion velocity. The diffusion terms are calculated using 10th-order central finite difference and are non-dimensionalized by the filtered scalar dissipation rate and the SGS variance, respectively. In the following we discuss the results for each major species mass fraction. We show the results for flame D with the filter size, Δ=3.0 mm (additional flame D results and some flame E results are given in the Supplemental materials). The results for $\Delta = 4.9$ mm are qualitatively similar and are not shown. Due to the space limitations we focus on the results involving Y_{CO_2} and Y_{CO}, which have the simplest and the most complex structures, respectively, and briefly discuss the results for the other species.

The FMDF of ξ, T and Y_{CO_2} appears to be largely limited to a two-dimensional manifold and has a similar shape to the FMDF of ξ & T due to the strong correlation between T and Y_{CO_2} (Figs. 1 and 2), since Y_{CO_2} is directly related to the heat release. Consequently, although there are four scalars in the mixing problem, i.e., ξ, T, Y_{CO_2}, and the co-flow, the SGS mixing is similar to three-scalar SGS mixing. Thus, the mixing problem for these scalars is a degenerated case. At $x/D = 7.5$ the flame is close to fully burning, with T and Y_{CO_2} not far from the equilibrium values. For small SGS variance, the FMDF is unimodal and is concentrated near the peak T and Y_{CO_2} (Fig. 1a). For large SGS variance, the FMDF is bimodal (Fig. 1b), indicating that the rich and lean mixtures in the SGS field (i.e., a grid cell) are essentially segregated. The difference between the ξ values of the two mixtures is greater than the reaction zone width in the ξ space, $\Delta\xi_R$ ($\approx$0.23), for the Sandia flames. Such a mixture fraction structure limits the reaction zones to thin diffusion layers, thereby resulting in laminar flamelets. For flame E both T and Y_{CO_2} are lower than those for flame D (Fig. S15b), and there is a relatively large probability of local extinction due to the higher scalar dissipation rate, but the results are otherwise similar to those for flame D. At $x/D = 15$ there is a significant number of local extinguished samples, with flame E having approximately five times that in flame D (Fig. S16b). At $x/D = 30$, the probability of local extinction is approximately two to three times lower than at $x/D = 15$ due to reignition as a result of the decay of the scalar dissipation rate (Fig. S3b).

The diffusion velocity streamlines for ξ, T and Y_{CO_2} are shown in Figs. 1 and 2. For small SGS variance the streamlines at $x/D = 7.5$ generally converge first to a one-dimensional manifold, which is the ridgeline of the FMDF, and then continue towards a stagnation point. The diffusion velocity magnitude is larger during the approach to the manifold, indicating that the approach to the manifold is a faster process than the convergence to the stagnation point. This trend can be understood largely in the context of quasi-equilibrium distributed reaction zones, in which reactive scalar diffusion is closely coupled to the diffusion of the mixture fraction dissipation [9]. At $x/D = 15$ (Fig. 2c) the streamline for the burning samples are similar to those at $x/D = 7.5$. For the samples at lower T and Y_{CO_2}, there is another

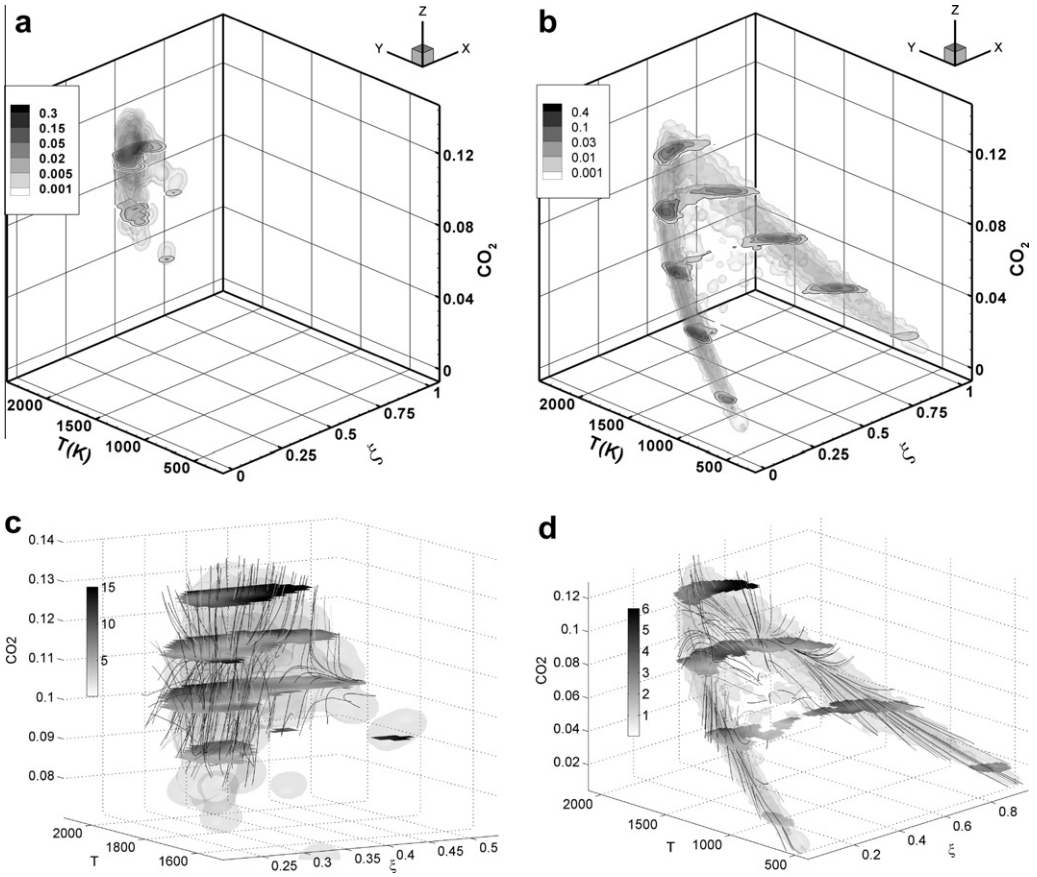

Fig. 1. FMDF and diffusion velocity streamlines for ξ, T and Y_{CO_2} at $x/D = 7.5$ in flame D. (a & c) small SGS variance ($\langle\langle\xi''^2\rangle_L\rangle = 0.0013$, $\langle\langle\xi''^2\rangle_L\rangle = 0.0272$); (b & d) large SGS variance ($\langle\langle\xi''^2\rangle_L = 0.066$). The grey scales on the horizontal planes represent the magnitude of the diffusion velocity vectors.

stagnation point near $\xi = 0.4$, $T = 1600K$, and $Y_{CO_2} = 0.075$ (0.4, 1600 K, 0.075). Here the mixing is primarily between the burning and extinguished samples. The results for $x/D = 30$ is similar to those at $x/D = 15$ (Fig. S3c).

For large SGS variance at $x/D = 7.5$ the streamlines for very rich ($\xi > 0.6$) and lean ($\xi < 0.2$) mixtures generally move along the FMDF (Fig. 1d) towards the stoichiometric mixture fraction. For strained flamelets the mixture fraction profiles have an approximately error-function shape (ramp-cliff structure). Thus, ξ diffuses towards the center of the profiles (appears to be near $\xi = 0.45$). For very rich and lean mixtures T and Y_{CO_2} depend approximately linearly on ξ; therefore, they diffuse along with ξ, resulting in straight diffusion streamlines along the ridgeline.

Near the peak T and Y_{CO_2} the ξ diffusion is small (close to the center of the error-function profiles). The T diffusion and Y_{CO_2} diffusion are negative due to the negative curvatures of their profiles (as a function of ξ) and the approximately linear ξ profiles. Consequently, the streamlines move towards lower T and Y_{CO_2} values. As the streamlines move towards lower temperatures, the scalar dissipation rate increases, corresponding to more strongly strained flamelets and higher diffusion. The largest magnitude of the diffusion velocity vector (≈6.0) occurs near $T = 1600$–1800 K and slightly to the rich side of ξ_s. Below this temperature range T and Y_{CO_2} profiles become broader (smaller curvatures) in the ξ space, resulting in lower T diffusion and Y_{CO_2} diffusion. There appears to be a stagnation point at (0.4, 1300 K, 0.058). Note that although this point appears to be the "center" of diffusion, it does not correspond to the conditional mean temperature and conditional mean Y_{CO_2} for this mixture fraction value. Since the FMDF is transported by both diffusion and reactions, their combined action keeps the FMDF in its manifold. Individually they generally transport the FMDF out of the manifold unless one of them is small. Near the maximum

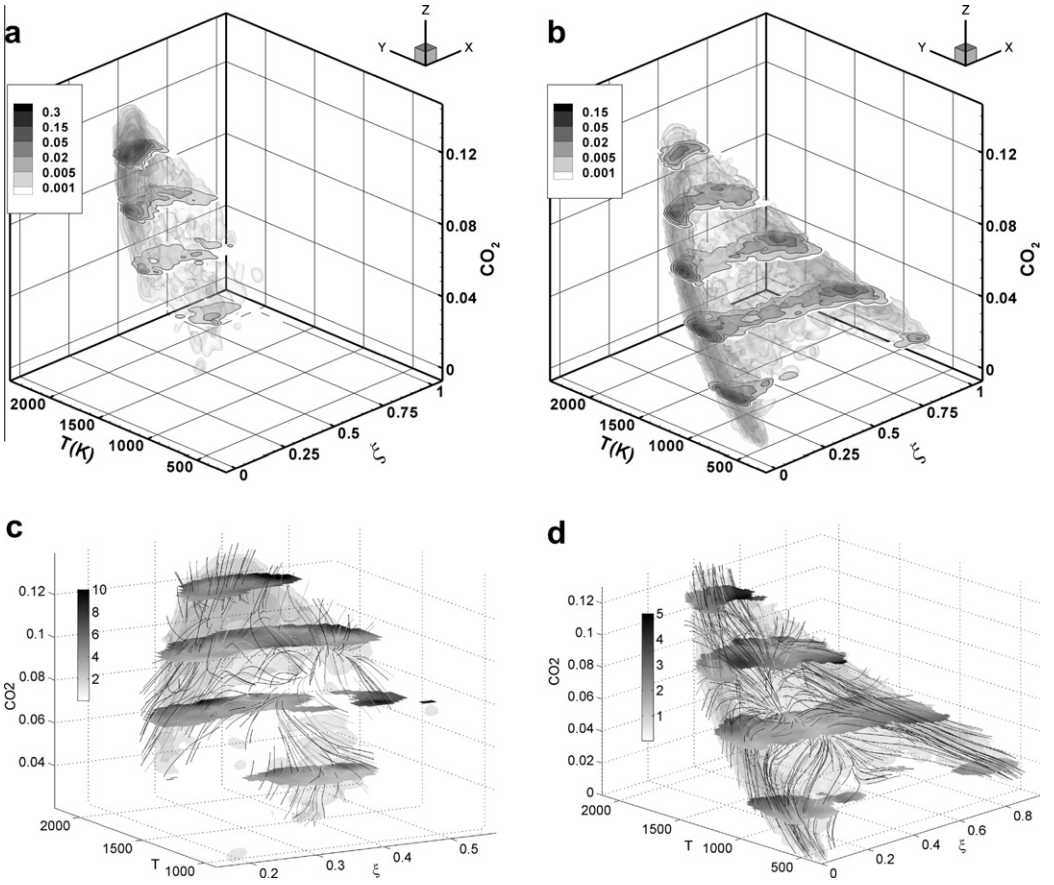

Fig. 2. FMDF and diffusion velocity streamlines for ξ, T and Y_{CO_2} at $x/D = 15$ in flame D. (a & c) small SGS variance ($\langle\langle\xi''^2\rangle_L\rangle = 0.003$, $\langle\langle\xi''^2\rangle_L\rangle = 0.0251$); (b & d) large SGS variance ($\langle\langle\xi''^2\rangle_L = 0.069$).

diffusion magnitude the reaction rates are also large, thus the diffusion streamlines move out of the FMDF manifold.

The streamlines starting from the very rich and lean regions turn near (0.27, 1600 K, 0.082) and near (0.55, 1600 K, 0.0760), respectively, where the inflection points of T and Y_{CO_2} profiles are located. Below these points the diffusion is dominated by mixing whereas above them the diffusion is strongly influenced by both mixing and reaction. This streamline pattern is also consistent with the structure of flamelets.

At $x/D = 15$, the overall diffusion pattern for the burning samples (Fig. 2d) is similar to that at $x/D = 7.5$. The largest magnitude of the diffusion velocity has decreased to approximately 4.0. For the extinguished samples the diffusion streamlines move primarily in the direction of mixture fraction towards $\xi \approx 0.4$, with only modest increases in T and Y_{CO_2}. The magnitude, however, is quite low (typically less than 1.0). These trends indicate that for these samples the ξ diffusion is initially much faster than T diffusion. Previous results [9] have shown that this trend is due to extinguished flamelets. Near $\xi = 0.4$ streamlines move largely in the direction of T and Y_{CO_2} towards higher values. For each flamelet, the T and Y_{CO_2} diffusion is negative at this mixture fraction. Thus, the observed positive T and Y_{CO_2} diffusion is likely due to the interaction between burning and extinguished flamelets resulting in diffusion along the iso-mixture fraction surface. At $x/D = 30$ the results (Fig. S3d) are similar to those at $x/D = 15$ with the maximum diffusion magnitude decreasing to 3.8. The results for flame E are qualitatively similar to those for flame D at $x/D = 15$ and 30 except the earlier onset of local extinction (Fig. S15-S17). The results for H_2O are similar to CO_2 and are not shown.

The FMDF and the conditionally filtered diffusion involving Y_{O_2} are shown with the ξ axis plotted differently for clarity. Due to partial premixing mixing, the FMDF at $x/D = 7.5$ (Figs. S7a-b) is similar to the inverted FMDF of ξ, T and Y_{CO_2}, with higher Y_{O_2} values for both lean and rich mixtures but low values near ξ_s. The FMDF,

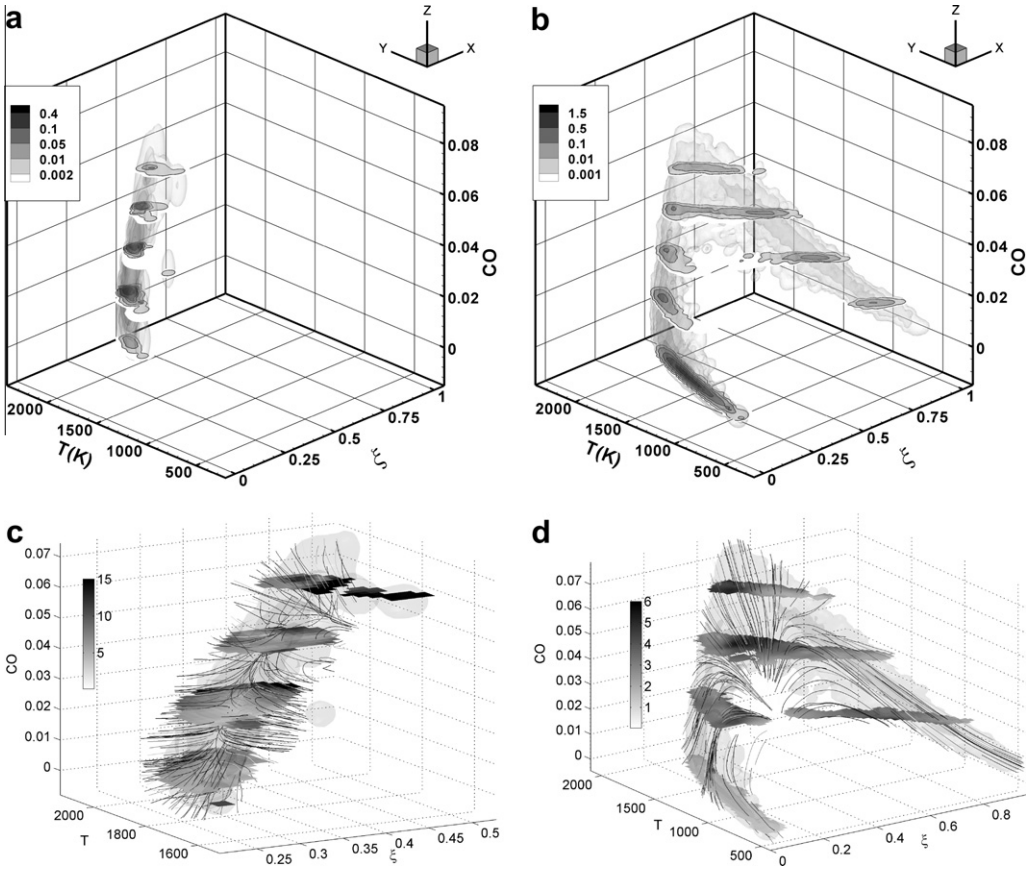

Fig. 3. FMDF and diffusion velocity streamlines for ξ, T and Y_{CO}. Conditions same as in Fig. 1.

although not in a plane, is largely limited to a two-dimensional manifold. At $x/D = 15$ (Fig. S8a), for small SGS variance the FMDF is again similar to the inverted FMDF containing Y_{CO_2}. For large SGS variance (Fig. S8b), the extent of the rich side is reduced due to consumption. There are some samples with higher Y_{O_2} at lower temperatures due to local extinction. At $x/D = 30$ the rich side has further diminished (Fig. S9b).

At $x/D = 7.5$ the diffusion streamline pattern (Fig. S7c-d) involving Y_{O_2} is similar to the inverted streamlines involving Y_{CO_2}. Moving downstream to $x/D = 15$, for small SGS variance, the streamlines converge to the stagnation points (Fig. S8c). For large SGS variance, the streamlines (Fig. S8d) are also similar to the inverted streamlines for Y_{CO_2}, but those on the rich side start from lower Y_{O_2} values than at $x/D = 7.5$. At $x/D = 30$, the streamlines start from even lower Y_{O_2} values (Fig. S9d).

The FMDF of ξ, T, and Y_{CH_4} at $x/D = 7.5$ is concentrated near equilibrium values (Fig. S10b). The CH_4 levels on the lean side are very low. At $x/D = 15$ the FMDF extends to higher Y_{CH_4} values and lower T values (Fig. S11b). The FMDF also appear to be limited to a plane. The diffusion streamlines have a similar structure to those for Y_{CO_2} (Fig. S11d). Near the peak temperature they move towards lower T and higher Y_{CH_4} values. The streamlines from the far rich and lean sides move along the FMDF. For the extinguished samples the streamlines move towards $\xi = 0.4$ and then converge to a stagnation point.

The FMDF for T and Y_{CO} at $x/D = 7.5$ are not far from the equilibrium values. For small SGS variance, the FMDF is concentrated on the lean side of the peak Y_{CO} (Fig. 3a). There is a sharp drop of Y_{CO} due to the consumption reactions. For large SGS variance, the FMDF consists of three segments, one on the rich side of the peak Y_{CO} and two on the lean side (Fig. 3b), connecting four vertices that are not in the same plane; therefore, unlike that of ξ, T and Y_{CO_2}, the FMDF of ξ, T and Y_{CO} must be represented in a three-dimensional scalar space. Thus, the mixing problem is non-degenerated. On the far rich side the FMDF ridgeline is largely a straight line, due to the low

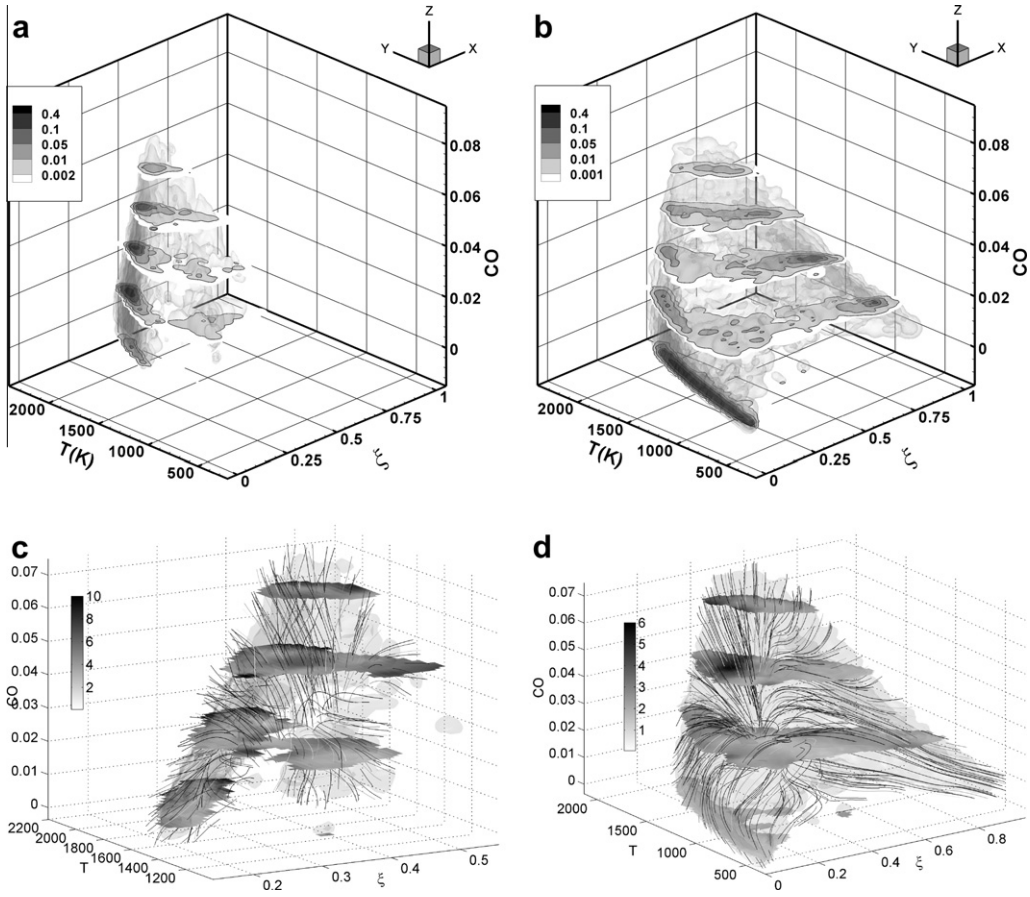

Fig. 4. FMDF and diffusion velocity streamlines for ξ, T and Y_{CO}. Conditions same as in Fig. 2.

reaction rates resulting in linear relationships among the scalars. The production rate of Y_{CO} is highest near the peak, and is balanced by the negative diffusion. Just to the lean side of the peak Y_{CO}, where the consumption rate is highest, Y_{CO} decreases rapidly to reach very low values at $\xi = 0.2$. Further to the lean side Y_{CO} remains low and T decreases linearly with ξ.

At $x/D = 15$ for small SGS variance, the FMDF is still largely concentrated on the lean side of the peak Y_{CO}, but extends to the rich side as well as regions of lower T and Y_{CO} due to local extinction (Fig. 4a). For large SGS variance the parts of the FMDF corresponding to the burning samples are similar to those at $x/D = 7.5$ (Fig. 4b). These samples and those with lower temperatures form a triangular pyramid-shaped FMDF manifold. A plane on the lean side (left plane) containing three vertices $(0.01, 378\ \mathrm{K}, 0.001)$, $(0.26, 1745\ \mathrm{K}, 0.001)$ and $(0.49, 1934\ \mathrm{K}, 0.07)$ is formed due to the rising Y_{CO} values resulting from the imbalance between Y_{CO} diffusion and the (reduced) CO consumption rate. These are flamelets that are strained or close to extinction. A front plane connecting the left plane and the ridgeline on the rich side is also formed. The elevated CO levels due to the diffusion and the reduced CO consumption result in similar profiles of Y_{CO} and T (hence the profiles are on the front plane). At this downstream location the FMDF values are low inside the pyramid.

At $x/D = 30$ the overall shape of the FMDF (Fig. S6a-b) is similar to that at $x/D = 15$. For large SGS variance, the pyramid appears to be filled to a larger extent. The elevated CO levels inside the pyramid provides the possibility of mixing between the rich mixtures at high temperatures and the lean mixtures at low temperatures. The SGS mixing is likely between burning and extinguished flamelets.

The diffusion streamlines for small SGS variance at $x/D = 7.5$ converge to a manifold and then to a stagnation point (Fig. 3c). At $x/D = 15$ (Fig. 4c) there is a second stagnation point at lower Y_{CO} values, towards which the streamlines converge. The results for $x/D = 30$ are similar.

For large SGS variance at $x/D = 7.5$ (Fig. 3d) near the peak Y_{CO}, the diffusion streamlines move largely towards lower T and Y_{CO} values. Here both the reaction rates and the negative diffusion are high and largely balance each other and their combined action transports the FMDF within the FMDF manifold. Thus, the diffusion alone transports the FMDF out of the manifold, as shown in Fig. 3d. The maximum diffusion magnitude ($\approx$6.0) occurs slight to the lean side of the peak Y_{CO}. On the far lean side and the far rich side the reaction rates are low, and the streamlines stay inside the FMDF manifold. On the lean side between 1000 K to 1500 K, the diffusion streamlines move towards higher Y_{CO} but remain at approximately the same T. Due to the high CO consumption rate in these mixtures, the streamlines tend to move out of the FMDF manifold. The streamlines then turn towards lower T and Y_{CO}, and converge to a stagnation point in the interior of the pyramid (not on the front or the back plane).

At $x/D = 15$ the streamline pattern for the burning samples are similar to that at $x/D = 7.5$ (Fig. 4d) with the maximum magnitude decreasing to approximately 4.0. For the extinguished samples, the streamlines from low T and Y_{CO} on the far lean side first move upward towards higher Y_{CO}. Here the reaction rates are low and the streamlines are located within the FMDF manifold (the left plane), which is generated by the diffusion. The streamlines then move towards ξ_s. On the rich side, the streamlines for the extinguished flamelets also move towards ξ_s, and together with those from the lean side forming the front plane. Since the reaction rates are low, the FMDF is transported in the direction of the streamlines. Near ξ_s the streamlines move towards the stagnation point at higher T and lower Y_{CO}. Again, for each flamelet the diffusion for both T and Y_{CO} is in the opposite direction of the streamlines. The diffusion here, therefore, is along the iso-mixture fraction surface (near ξ_s), indicating diffusion among burning and extinguished flamelets. At $x/D = 30$, the overall streamline pattern is similar to that at $x/D = 15$ (Fig. S6c-d) with the maximum magnitude further decreasing to 3.0. The results for H_2 are generally similar to those of CO. One difference is that at $x/D = 15$ (Fig. S14), the FMDF is broader than that of CO potentially due to higher noise as well as possible differential diffusion effects resulting from the higher diffusion coefficient of H_2.

The Sandia flames are piloted flames, and the pilot can play a role in the mixing process. While some previous studies suggested that the pilot gas had already been thoroughly mixed at x/d=7.5, we have observed some possible influence of the pilot on scalar dissipation and the diffusion streamlines on the rich side at x/d=7.5 and 15 [12,9]. The impact on the lean side, where most of the interesting phenomena in present study are observed, was found to be negligible. Thus, the pilot does not have a strong impact on the results of this study.

The results show that the SGS mixing of Y_{CO_2} and that of Y_{CO} have significantly different characteristics. Being strongly correlated with the temperature, the SGS mixing of Y_{CO_2} is similar to that of the temperature. The four-scalar (ξ, T, Y_{CO_2}, and co-flow ($1 - \xi$)) SGS mixing problem is similar to that of the three scalar (ξ, T, and co-flow) SGS mixing, and therefore, is a degenerated case. On the other hand, the SGS mixing of ξ, T, Y_{CO}, and co-flow is more complex because Y_{CO} is depleted rapidly towards the lean side, resulting in a FMDF with four vertices that must be represented in a three-dimensional scalar space. Thus, the SGS mixing problem is non-degenerated. From a more general point of view, the different SGS mixing characteristics of Y_{CO_2} and Y_{CO} are a result of the different mixing configurations, i.e., the spatial relationships among the scalars in physical space, which are closely tied to the chemistry: In the Sandia flames the major species can be divided into several categories: CO_2 and H_2O, CO and H_2, and CH_4, and O_2, each having a different spatial relationship with the mixture fraction, the temperature, and the co-flow. Except CO and H_2, the FMDFs for all the species have vertices near the peak temperature indicating relatively simple mixing configurations. In flames with more complex chemistry, additional mixing configurations may exist, resulting in different SGS mixing characteristics.

4. Conclusions

We used data obtained in turbulent partially premixed flames (Sandia flames D and E) to study the influence of the SGS mixture fraction structure on the SGS mixing of the mixture fraction, temperature, and species mass fractions. The Favre filtered mixture fraction and the Favre SGS scalar variance were used as conditioning variables for analyzing the scalar filtered mass density function and the conditionally filtered diffusion. The main findings are:

- The SGS mixing regimes for the mixture fraction result in qualitatively different characteristics of the SGS mixing of species mass fractions.
- For small SGS variance, the FMDF is unimodal. For samples close to equilibrium the diffusion streamlines generally converge to a manifold and then move towards a stagnation point. At lower temperatures, the streamlines converge to another manifold and stagnation

point at approximately 1600 K, due to the SGS mixing between burning and extinguished samples.
- For large SGS variance, the FMDF is bimodal. The diffusion streamline pattern is consistent with burning and extinguished flamelets.
- There is evidence suggesting flamelet-flamelet interactions, resulting diffusion along the stoichiometric mixture fraction surface.
- The mixing configuration of the mixture fraction, temperature and a species mass fraction, which results from the turbulence-chemistry interaction, has a strong influence on the SGS mixing of the species mass fraction. Due to its strong correlations with the temperature, the SGS mixing of Y_{CO_2} (and Y_{H_2O}) is similar to that of temperature. Thus, the SGS mixing of ξ, T, and Y_{CO_2} can largely be represented by a two-dimensional manifold, and therefore is degenerated. On the other hand, the rapid depletion of Y_{CO} on the lean side results in a more complex mixing configuration, and the SGS mixing of ξ, T, and Y_{CO} must be represented by a three-dimensional manifold and is non-degenerated.

The present study shows that both the SGS mixing regimes and the SGS mixing configurations have a strong influence on the SGS mixing of the species mass fractions. The results present a challenging test for SGS mixing models.

Acknowledgments

We thank Dr. Robert Barlow and Professor Adonios Karpetis for providing the Sandia flame data. This work was supported by AFOSR under Grant No. F-9550-06-1-0036 and the National Science Foundation under Grant No. CBET-0651174.

Appendix A. Supplementary data

Supplementary data associated with this article can be found, in the online version, at http://dx.doi.org/10.1016/j.proci.2012.05.017.

References

[1] S.B. Pope, Computations of turbulent combustion: progress and challenges, in: *Proceedings of the 23rd Symposium (International) on Combustion*, 1990, pp. 591–612.
[2] P.J. Colucci, F.A. Jaberi, P. Givi, S.B. Pope, *Phys. Fluids* 10 (1998) 499–515.
[3] C. Tong, *Phys. Fluids* 13 (2001) 2923–2937.
[4] A.G. Rajagopalan, C. Tong, *Phys. Fluids* 15 (2003) 227–244.
[5] D. Wang, C. Tong, *Phys. Fluids* 14 (2002) 2170–2185.
[6] D. Wang, C. Tong, S.B. Pope, *Phys. Fluids* 16 (2004) 3599–3613.
[7] D. Wang, C. Tong, *Proc. Combust. Inst.* 30 (2005) 567–574.
[8] D. Wang, C. Tong, R.S. Barlow, A.N. Karpetis, *Proc. Combust. Inst.* 31 (2007) 1533–1541.
[9] J. Cai, R.S. Barlow, A.N. Karpetis, C. Tong, *Proc. Combust. Inst.* 33 (2011) 1505–1513.
[10] A.N. Karpetis, R.S. Barlow, *Proc. Combust. Inst.* 30 (2005) 665–672.
[11] R.S. Barlow, A.N. Karpetis, *Flow, Turb. Combust.* 72 (2004) 427–448.
[12] J. Cai, R.S. Barlow, A.N. Karpetis, C. Tong, *Flow, Turb. Combust.* 85 (2010) 309–332.
[13] G. Wang, A.N. Karpetis, R.S. Barlow, *Combust. Flame* 148 (2007) 62–75.
[14] J. Cai, M.J. Dinger, W. Li, C.D. Carter, M.D. Ryan, C. Tong, *J. Fluid Mech.* 685 (2011) 495–531.
[15] R.S. Barlow, J.H. Frank, A.N. Karpetis, J.-Y. Chen, *Combust. Flame* 143 (2005) 433–449.